Available online at www.sciencedirect.com

SciVerse ScienceDirect

Ceramics International 39 (2013) 1129–1134

CERAMICS INTERNATIONAL

www.elsevier.com/locate/ceramint

Y_2O_3:Yb,Tm and Y_2O_3:Yb,Ho powders for low-temperature thermometry based on up-conversion fluorescence

V. Lojpur[a], M. Nikolic[b], L. Mancic[a], O. Milosevic[a], M.D. Dramicanin[b,*]

[a]*Institute of Technical Sciences of SASA, K. Mihailova 35/IV, Belgrade, Serbia*
[b]*Vinča Institute of Nuclear Science, University of Belgrade, P.O. Box 522, Belgrade, Serbia*

Received 15 June 2012; received in revised form 9 July 2012; accepted 9 July 2012
Available online 20 July 2012

Abstract

Recently, trivalent rare earth doped materials have received significant attention due to the strong temperature dependence of the fluorescence emission of these materials, which can be useful in temperature sensing. Here, we investigated Y_2O_3 ceramic powders doped with Yb^{3+} and co-doped with either Tm^{3+} or Ho^{3+}. The powders were obtained *via* spray pyrolysis at 900 °C and additionally thermally treated at 1100 °C for 24 h. Structural characterization using X-ray powder diffraction confirmed the cubic bixbyte structure. Scanning electron microscopy (SEM) revealed that the particles exhibit a uniform spherical morphology. The up-conversion emissions were measured using laser excitation at 978 nm, resulting in the following transitions: blue emission in the range of 450–500 nm, weak red emission in the range of 650–680 nm and near infrared emission in the range of 765–840 nm for Tm^{3+}, as well as green emission centered at 550 nm and weak near infrared emission at 755 nm for the Ho^{3+} ions. In addition, the temperature dependence of the fluorescence intensity ratios of different Stark components was analyzed in the range of 10–300 K. Significant temperature sensitivity was detected for several components, with the largest value of 0.097 K^{-1} related to the intensity ratio of I_{536} and I_{772} emissions observed for the Y_2O_3:Yb,Ho powder.

Keywords: D. Y_2O_3; Spray pyrolysis; Thermometry; Up-conversion

1. Introduction

Phosphors are materials composed of a transparent host and an activator, typically a small quantity of a transition metal or a rare earth ion [1]. After absorbing a specific form of energy, these materials emit light in the ultraviolet (UV), visible (VIS) or infrared (IR) spectral regions. Rare earth (RE^{3+}) ion doped materials have been widely used as fluorescent and light-emitting diodes (LED), biological labels, lasers and components in a variety of display technologies [2–5]. Because the absorption and emission properties of phosphors change with temperature, they could find applications in optical temperature sensing devices [6]. Phosphor thermometry represents an optical technique for surface temperature measurements that is based on the time and temperature dependence of phosphorescence intensity. The fluorescent intensity ratio (FIR) is the foremost technique used to reduce the influence of measurement conditions and improve the sensitivity of the measurement [7,8]. This simple, non-contact and precise method is applicable over a wide temperature range (from 10 K to 2000 K) and involves the comparison of intensities of two emission lines or areas in photoluminescent spectra.

Using this technique, RE^{3+} ion doped bulk and nanomaterials have been prepared in the literature, and some have been used as temperature sensors. For example, the high temperature sensing behavior of Er^{3+} or Nd^{3+} doped strontium barium niobate ceramic glasses was reported in a study [9], whereas Nikolic et al. discussed a possible application of the FIR method for Sm^{3+} doped $GdVO_4$ phosphors [10]. Additionally, it was shown that the same technique is useful for the determination of up-conversion in Er^{3+}/Yb^{3+} co-doped Gd_2O_3 [11] and $Er^{3+}/Yb^{3+}/Li^{+}$ doped ZrO_2 [12].

The synthesis of new rare-earth sesquioxides has generated significant interest due to their excellent chemical

*Corresponding author. Tel./fax: +381 11 3408 678.
E-mail address: dramican@vinca.rs (M.D. Dramicanin).

0272-8842/$ - see front matter © 2012 Elsevier Ltd and Techna Group S.r.l. All rights reserved.
http://dx.doi.org/10.1016/j.ceramint.2012.07.036

stability, good thermal conductivity and transparency to infrared radiation. In particular, Y_2O_3-based ceramics have been used as efficient host matrix materials because of their high energy band gap (5.8 eV), broad optical spectra, refractive index of ~2, low phonon energy (~ 430–550 cm^{-1}), high melting point (~2450 °C), and low thermal expansion coefficient [13]. In their pure form, Y_2O_3 materials are used as cutting tools, crucibles for the melting of metals, and nozzles for jet-casting, among other uses. Uniform material doping is usually achieved using wet-chemistry synthetic techniques, including hydrothermal synthesis, emulsion liquid membrane, sol–gel, homogenous precipitation, and the polymer complex solution method, among others [14–18]. Spray pyrolysis is also a well-known technique for the synthesis of nanostructured particles with a specific size and morphology, as well as a uniform distribution of luminescent centers within the host, resulting in enhanced optical properties [19].

Herein, we discuss the structural and optical characterizations of Y_2O_3:Yb^{3+},Ho^{3+} and Y_2O_3:Yb^{3+},Tm^{3+} powders synthesized using the spray pyrolysis method. We also examine their emission properties in the temperature range of 10–300 K to explore for the first time the possibility of utilizing these materials in low-temperature sensing applications.

2. Experimental

Yttrium oxide powders doped with either Yb^{3+},Tm^{3+} or Yb^{3+},Ho^{3+} were synthesized *via* spray pyrolysis from 0.1 M precursor solutions. The precursor solutions were composed of $Y(NO_3)_3 \cdot 6H_2O$, $Yb(NO_3)_3 \cdot 5H_2O$, Tm_2O_3 and Ho_2O_3 in appropriate stoichiometric ratios for generating the following compositions: $Y_{1.89}Yb_{0.1}Tm_{0.02}O_3$ and $Y_{1.89}Yb_{0.1}Ho_{0.02}O_3$. The nitrate salts were dissolved in distilled water, whereas the oxides were dissolved in hot nitric acid. The resulting precursors (containing either Tm^{3+} or Ho^{3+}) were atomized at 1.7 MHz using an ultrasonic aerosol generator (Profi Sonic-Prizma, Serbia) and then injected into a heated quartz tube by air flow (1.6 dm^3/min). Aerosol decomposition was performed at 900 °C. The droplet/particle residence time in the reactor was 21 s. The resulting powders were collected at the end of a quartz tube and thermally treated at 1100 °C for 24 h.

The phase composition was determined by X-ray powder diffraction (XRPD) using a Philips 1050 diffractometer, operating with a Cu K_α radiation source. The 2θ was analyzed in the range of 10–100° with a step scan of 0.02 and a counting time of 12 s per step. The powder morphology was investigated by scanning electron microscopy (Tescan Vega TS 5130MM). Photoluminescence measurements were performed on a spectrofluorometer equipped with an optical parametric oscillator excitation source (EKSPLA NT 342, in the emission range of 210–2300 nm), a Cryostat (Advance Research Systems DE202-AE with a Lakeshore model 331 controller), a spectrograph FHR 1000 (Horiba Jobin-Yvon, 300 groove/mm grating) and an ICCD detector (Horiba Jobin-Yvon 3771).

3. Results and discussion

The powders obtained *via* spray pyrolysis exhibit a cubic crystal structure, s.g. *Ia-3*, that corresponds to the $Y_{1.88}Yb_{0.12}O_3$ compound (PDF 87-2368). Fig. 1 provides the X-ray diffraction pattern of $Y_{1.89}Yb_{0.1}Ho_{0.02}O_3$ annealed at 1100 °C for 24 h. Narrow diffraction lines with high intensities indicate good powder crystallinity.

The typical morphology of particles synthesized using the spray pyrolysis method is shown in Fig. 2. The resulting particles are spherical, sub-micronic in size and un-agglomerated. A closer inspection reveals that the particles are composed of smaller primary subunits, which give rise to a grainy surface appearance. Significant particle porosity is also observed. The spherical shape of the

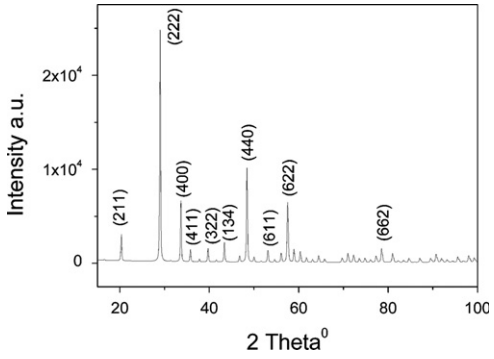

Fig. 1. X-ray diffraction pattern of Y_2O_3:Yb^{3+},Ho^{3+} powder annealed at 1100 °C for 24 h.

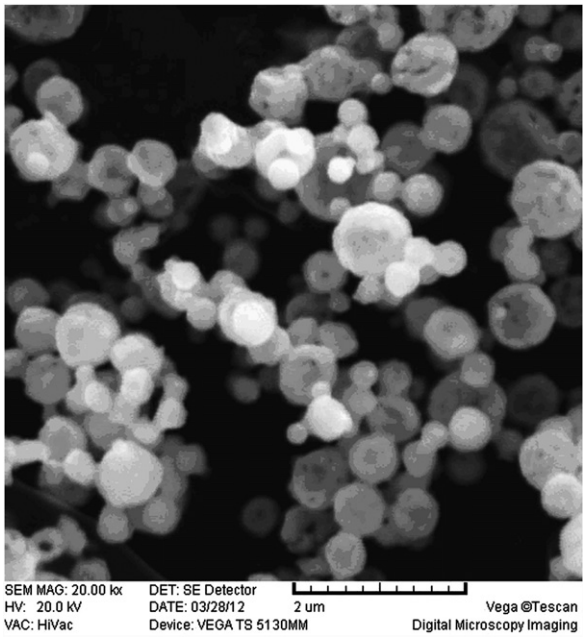

Fig. 2. SEM image of Y_2O_3:Yb^{3+},Ho^{3+} particles synthesized through spray pyrolysis.

particles is preserved even after a thermal treatment at 1100 °C for 24 h, although in rare cases, the formation of "necks" between particles is observed. Due to contact deficiency between primary subunits throughout the entire volume of spherical particles, the opening of pores and the generation of sponge-like structures are observed with the larger particles.

The up-conversion emission spectra of Y_2O_3:Yb^{3+},Tm^{3+} were obtained using 978 nm laser excitation in the range of 10–300 K. As shown in Fig. 3, three emission bands are observed: a blue emission band in the range of 450–500 nm, a weak red emission band in the range of 650–680 nm, and a near infrared emission band in the range of 765–840 nm. The observed emission peaks are assigned to the 4f electron transitions of Tm^{3+}, including the blue ($^1D_2 \rightarrow {}^3F_4$, $^1G_4 \rightarrow {}^3H_6$), the weak red ($^1G_4 \rightarrow {}^3F_4$, $^3F_{2,3} \rightarrow {}^3H_6$) and the near infrared ($^1D_2 \rightarrow {}^3F_3$, $^1G_4 \rightarrow {}^3H_6$, $^3H_4 \rightarrow {}^3H_6$) emissions. The emission intensities of red bands increase with decreasing temperature, whereas the blue and near infrared bands do not exhibit any obvious trends with varying temperature.

The up-conversion emission spectra of Y_2O_3:Yb^{3+},Ho^{3+} were obtained using 978 nm laser excitation in the range of 10–300 K. As shown in Fig. 4, two emission peaks are observed: a strong green emission peak centered at 550 nm and weak near infrared peak at 755 nm. The observed peaks are assigned to the 4f electron transitions of Ho^{3+}, including multiple transitions for green ($^5F_4$, $^5S_2 \rightarrow {}^5I_8$) and near infrared

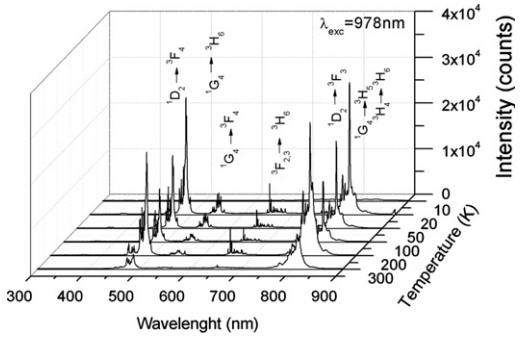

Fig. 3. Up-conversion spectra of Y_2O_3:Yb^{3+},Tm^{3+} in VIS and IR regions.

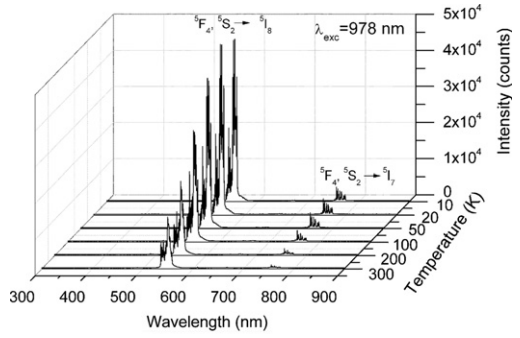

Fig. 4. Up-conversion spectra of Y_2O_3:Yb^{3+},Ho^{3+} in VIS and IR regions.

($^5F_4$, $^5S_2 \rightarrow {}^5I_7$) emissions. Both emissions exhibit the same trends with increasing temperature, wherein the intensity significantly increases with decreasing temperature.

It is well known that for an ensemble of ions doped in a host material, the fluorescence intensity from a specific energy level depends on a number of parameters, such as the host material, the particular energy level of interest, the dimensions of the doped material and the excitation method employed. Thermally induced changes in fluorescence intensity usually arise from the temperature dependence of non-radiative rates of energy levels of interest or, in some cases, of other energy levels of the ion [20]. The temperature-dependent ratio of emissions from different energy levels may provide a method for measuring the temperature that is insensitive to changes in excitation intensity. For low temperature sensors, emissions from closely spaced energy levels are of particular interest. In these systems, the thermal occupation of levels above the ground or excited states can take place, and the relative population of these levels follows a Boltzmann type population distribution.

In the case of Y_2O_3:Yb^{3+},Tm^{3+} the temperature dependences of emissions at 815 nm, 656 nm, 460 nm and 454 nm were monitored, and a schematic representation of the transitions related to these emissions ($^1G_4 \rightarrow {}^3H_6$, $^1G_4 \rightarrow {}^3F_4$, $^1G_4 \rightarrow {}^3H_6$, $^1D_2 \rightarrow {}^3F_4$, respectively) is provided in Fig. 5a.

Because thermalization (rapid phonon-induced transitions) occurs between the Stark components of the excited levels, the emitted intensities are proportional to the population of each energy level, $I \propto N$, as shown in Fig. 5b:

$$N_a = N_a'' \exp(-\Delta E_a/kT),$$

$$N_b = N_b'' \exp(-\Delta E_b/kT),$$

where ΔE_a and ΔE_b are the energy differences of Stark components of excited states a and b, respectively, k is the Boltzmann constant and T is the temperature. Accordingly, the ratio of the fluorescence intensities of emissions from excited levels a to b can be represented in the following manner:

$$\mathrm{FIR} = \frac{I_a}{I_b} = \frac{N_a''}{N_b''} = C \exp(-(\Delta E_a - \Delta E_b)/kT), \quad (1)$$

where C is a constant that depends on spontaneous emission rates, the degeneracy of energy levels and emission energies.

Fig. 6 provides the experimentally derived FIR (symbols) of emission at 815 nm relative to emissions at 454 nm, 460 nm and 656 nm (black, red and green symbols, respectively). Solid lines represent the FIRs obtained by fitting the experimental data with Eq. (1). The fitting results are summarized in Table 1, together with the maximum sensitivity values (S_{max}), which are calculated from the first derivative of FIR as a function of temperature. The change in the FIR value per temperature unit is illustrated in Fig. 7. At temperatures of 270, 178 and 290 K, the sensitivity of Tm^{3+} exhibited maximum values of 0.078, 0.067 and

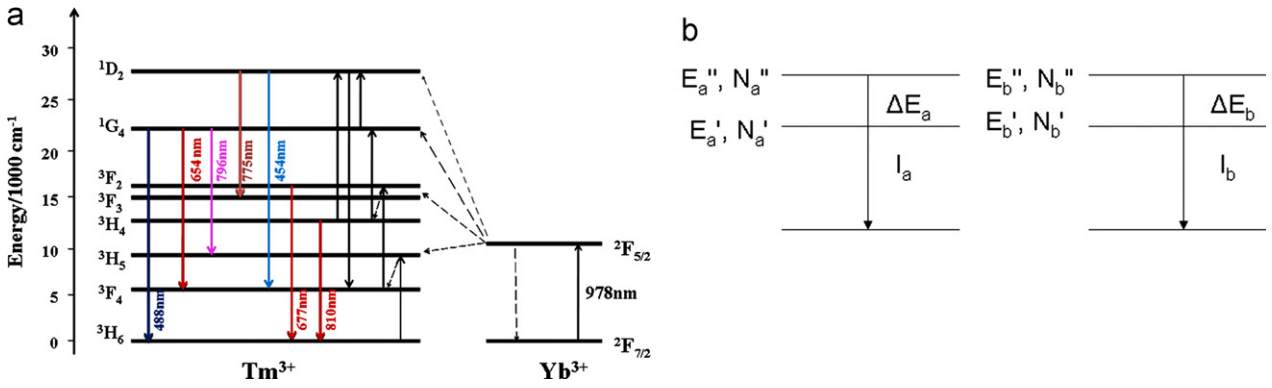

Fig. 5. (a) Energy level diagrams of Yb^{3+} and Tm^{3+} ions following excitation at 978 nm. (b) A simplified diagram of transitions from the two excited states with a large energy difference.

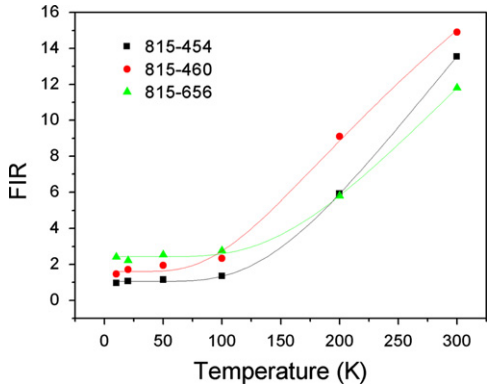

Fig. 6. Intensity ratio of Y_2O_3:Yb^{3+},Tm^{3+} emission at 815 nm relative to emissions at 454 nm, 460 nm and 656 nm (black, red and green symbols, respectively). The experimental data are represented as symbols, whereas the theoretical curves were obtained using Eq. (1) and are represented with solid lines. (For interpretation of the references to color in this figure legend, the reader is referred to the web version of this article.)

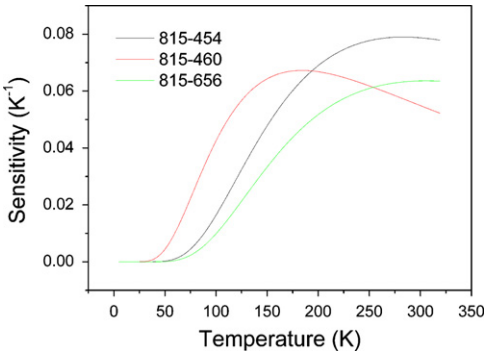

Fig. 7. Temperature dependence sensitivity of FIRs in Y_2O_3:Yb^{3+},Tm^{3+} with emission at 815 nm relative to emissions at 454 nm, 460 nm and 656 nm (black, red and green lines, respectively). (For interpretation of the references to color in this figure legend, the reader is referred to the web version of this article.)

Table 1
Fitting results of the experimentally obtained FIRs for Y_2O_3:Yb^{3+},Tm^{3+}.

FIR	C	$\Delta E_a - \Delta E_b$ (cm^{-1})	S_{max} (K^{-1})	R_{chi}
I_{815}/I_{454}	82.76	394	0.078	0.9997
I_{815}/I_{460}	45.88	257	0.067	0.9959
I_{815}/I_{656}	71.85	425	0.064	0.9979

0.064 K^{-1} for the 815/454, 815/440 and 815/656 emissions ratios, respectively.

For the Y_2O_3:Yb^{3+},Ho^{3+} system, the temperature dependence of green ($^5F_4$, $^5S_2 \rightarrow {}^5I_8$) and near infrared ($^5F_4$, $^5S_2 \rightarrow {}^5I_7$) emissions is shown in Fig. 8a. In this case, the emissions occur from two very closely separated levels ($^5F_4$ and $^5S_2$) by an energy difference of approximately 120 cm^{-1} [21] between the $^5I_7$ and $^5I_8$ lower and ground states. Therefore, the FIR can be analyzed using a four-level scheme presented in Fig. 8b, as introduced by Haro-González et al. [8].

The emission from two adjacent excited states to lower states a and b, I_a and I_b, can be described by the following relations:

$$I_a = I_a^{''} + I_a^{'} = N'' \omega_a^{''} g'' (h\nu)^{''} + N' \omega_a^{'} g' (h\nu)',$$

$$I_b = I_b^{''} + I_b^{'} = N'' \omega_b^{''} g'' (h\nu)^{''} + N' \omega_b^{'} g' (h\nu)',$$

where N is the population of the excited state, ω is the spontaneous emission rate, g is the degeneracy of the level and $(h\nu)$ is the transition energy. By taking into account that

$$N^{''} = N' \exp(-(E^{''} - E')/kT) = N' \exp(-\Delta E/kT),$$

the equation that describes the FIR in this case becomes

$$\mathrm{FIR} = \frac{I_a}{I_b} = \frac{1 + C_1 \exp(-\Delta E/kT)}{C_2 + C_3 \exp(-\Delta E/kT)}, \quad (2)$$

where C_1, C_2 and C_3 are constants that depend on spontaneous emission rates, degeneracy of the energy levels and emission energies.

Fig. 9 provides the experimentally derived FIRs (symbols) of emission at 536 nm relative to emissions at 758 nm, 764 nm and 772 nm (black, red and green symbols, respectively). Solid lines represent FIRs obtained by fitting the experimental data with Eq. (2). The fitting

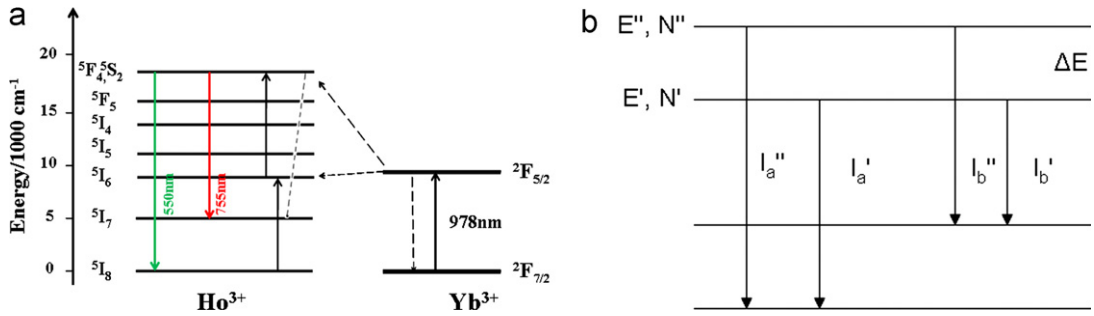

Fig. 8. Energy level diagrams of Yb^{3+} and Ho^{3+} ions following excitation at 978 nm (a). A four-level simplified diagram of transitions from adjacent excited levels to two lower levels (b).

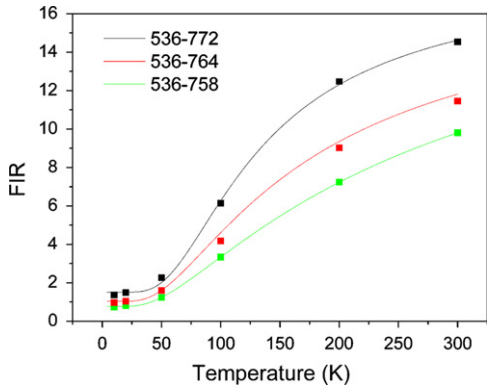

Fig. 9. Intensity ratio of Y_2O_3:Yb^{3+},Ho^{3+} emission at 536 nm relative to 758 nm, 764 nm and 772 nm emissions (black, red and green symbols, respectively). The experimental data are represented by symbols, whereas the theoretical curves were obtained using Eq. (2) and are represented with solid lines. (For interpretation of the references to color in this figure legend, the reader is referred to the web version of this article.)

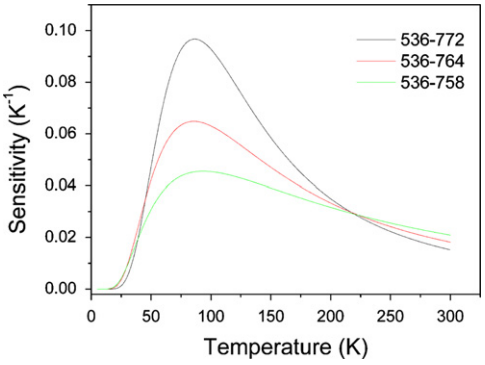

Fig. 10. The temperature dependence of sensitivity for FIRs in Y_2O_3:Yb^{3+},Ho^{3+} with emission at 536 nm relative to emissions at 758 nm, 764 nm and 772 nm emissions (black, red and green symbols, respectively). (For interpretation of the references to color in this figure legend, the reader is referred to the web version of this article.)

Table 2
Fitting results of the experimentally obtained FIRs for Y_2O_3:Yb^{3+},Ho^{3+}.

FIR	C_1	C_2	C_3	ΔE (cm^{-1})	S_{max} (K^{-1})	R_{chi}
$I_{536.5}/I_{758}$	11.94	1	0.37	114	0.046	0.9999
$I_{536.5}/I_{764.8}$	25.55	1	0.46	131	0.065	0.9994
$I_{536.5}/I_{772.6}$	73.34	1	3.09	170	0.097	0.9980

results are summarized in Table 2, together with maximum sensitivity values, as shown in Fig. 10. At temperatures of 85, 84 and 90 K, the sensitivity of Ho^{3+} exhibited maximum values of 0.097, 0.065 and 0.046 K^{-1} for emissions at 536/772, 536/764 and 536/758, respectively. It should be noted that the observed sensitivity is 30 times higher than those reported in the literature for the Er^{3+} and Ho^{3+} co-doped fluoroindate glasses [8].

Moreover, the sensitivity of both systems is significant enough for thermometry applications in the range of 10–300 K.

4. Conclusion

Yttrium oxide powders doped with either Yb^{3+},Tm^{3+} or Yb^{3+},Ho^{3+} were synthesized *via* the spray pyrolysis method. Spherical, sub-micrometer, un-agglomerated porous particles, composed of smaller primary subunits, exhibit a significant temperature sensitivity of up-conversion emission. In the case of Y_2O_3:Yb^{3+},Tm^{3+}, the temperature dependence of the emission intensity ratios of excited states with a large energy difference is due to the thermalization between the Stark components in the excited states. In the case of Y_2O_3:Yb^{3+},Ho^{3+}, emissions occur from adjacent excited states to two lower states, so the temperature dependence of the emission intensity ratios is a consequence of the thermalization between adjacent excited states. The observed temperature sensitivity of both systems is significant enough for thermometry applications in the range of 10–300 K.

Acknowledgments

This research is financially supported by the Projects 45020 and 171022 of the Ministry of Science and Education of the Republic of Serbia.

References

[1] J. Brubach, T Kissel, M Frotscher, M Euler, B Albert, A Dreizler, A survey of phosphors novel for thermometry, Journal of Luminescence 131 (2011) 559–564.

[2] F. Wang, X.G. Liu, Up-conversion multicolor fine-tuning: visible to near-infrared emission from lanthanide-doped $NaYF_4$ nanoparticles, Journal of the American Chemical Society 130 (2008) 5642–5643.
[3] H. Eilers, Effect of particle/grain size on the optical properties of Y_2O_3:Er,Yb, Journal of Alloys and Compounds 474 (2009) 569–572.
[4] F. Vetrone, J.C. Boyer, J.A. Capobianco, A. Speghini, M. Bettinelli, Significance of Yb^{3+} concentration on the up-conversion mechanisms in co-doped Y_2O_3:Er^{3+}, Yb^{3+} nanocrystals, Journal of Applied Physics 96 (2004) 661–667.
[5] X.X. Luo, W.H. Cao, Up-conversion luminescence of holmium and ytterbium co-doped yttrium oxysulfide phosphor, Materials Letters 61 (2007) 3696–3700.
[6] S.A. Wade, S.F. Collins, G.W. Baxter, Fluorescence intensity ratio technique for optical fiber point temperature sensing, Journal of Applied Physics 94 (2003) 4743–4757.
[7] N. Ishiwada, T. Ueda, T. Yokomori, Characteristics of rare earth (RE = Eu, Tb, Tm)-doped Y_2O_3 phosphors for thermometry, Journal of Biological Chemistry 26 (2011) 381–389.
[8] P. Haro-González, S.F. León-Luis, S. González-Pérez, I.R. Martín, Analysis of Er^{3+} and Ho^{3+} codoped fluoroindate glasses as wide range temperature sensor, Materials Research Bulletin 46 (2011) 1051–1054.
[9] P. Haro-González, I.R. Martín 1, L.L. Martín Sergio, F. León-Luis 1, C. Pérez-Rodríguez, V. Lavín, Characterization of Er^{3+} and Nd^{3+} doped strontium barium niobate glass ceramics temperature sensors, Optical Materials 33 (2011) 742–745.
[10] M.G. Nikolic, D.J. Jovanovic, V Đordjevic, Z Antic, R.M. Krsmanovic, M.D. Dramicanin, Thermographic properties of Sm^{3+}-doped $GdVO_4$ phosphor, Physica Scripta T149 (2012) 014063.
[11] S.K. Singh, K. Kumar, S.B. Rai, Er^{3+}/Yb^{3+} co-doped Gd_2O_3 nanophosphor for optical thermometry, Sensors and Actuators A: Physical 149 (2009) 16–20.
[12] L. Liu, Y. Wang, X. Zhang, K Yang, Y. Bai, C Huang, Y. Song, Optical thermometry through green and red up-conversion emissions in $Er^{3+}/Yb^{3+}/Li^{+}$:ZrO_2 nanocrystals, Optics communications 284 (2011) 1876–1879.
[13] A. Martinez, J. Morales, L.A. Diaz-Torres, P. Salas, E. De la Rosa, J. Oliva, H. Desirena, Green and red up-converted emission of hydrothermal synthesized Y_2O_3: Er^{3+}–Yb^{3+} nanophosphors using different solvent ratio conditions, Materials Science Engineering B 174 (2010) 164–168.
[14] G. De, W. Qin, J. Zhang, J. Zhang, Y. Wang, C. Cao, Y. Cui, Up-conversion luminescence properties of Y_2O_3:Yb^{3+},Er^{3+} nanostructures, Journal of Luminescence 119 (2006) 258–263.
[15] T. Hirai, T. Orikoshi, I. Komasawa, Preparation of Y_2O_3:Yb,Er infrared-to-visible conversion phosphor fine particles using an emulsion liquid membrane system, Chemistry of Materials 14 (2002) 3576–3583.
[16] D. Solis, T Lopez-Luke, E. De la Rosa, P Salas, C. Angeles-Chavez, Surfactant effect on the up-conversion emission and decay time of ZrO_2:Yb–Er nanocrystals, Journal of Luminescence 129 (2009) 449–455.
[17] M. Xing, W. Cao, H. Zhong, Y. Zhang, X. Luo, Y. Fu, W. Fei, T. Pang, X. Yang, Synthesis and up-conversion luminescence properties of monodisperse Y_2O_3:Yb,Ho spherical particles, Journal of Alloys and Compounds (2011) 5725–5730.
[18] R.M. Krsmanovic, Z. Antic, B. Bartova, M.G. Brik, M.D. Dramicanin, Fabrication of polycrystalline $(Y_{0.7}Gd_{0.3})_2O_3$:Eu^{3+} ceramics: the influence of initial pressure and sintering temperature on its morphology and photoluminescence activity, Ceramics International 38 (2012) 1303–1313.
[19] O. Milosevic, L. Mancic, M.E. Rabanal, L.S. Gomez, K. Marinkovic, Aerosol route in processing of nanostructured functional materials, KONA: Powder and Particle Journal 27 (2009) 84–106.
[20] S.A. Wade, S.F. Collins, G.W. Baxter, Fluorescence intensity ratio technique for optical fiber point temperature sensing, Journal of Applied Physics 94 (2003) 4743–4755.
[21] I.R. Martín, V.D. Rodríguez, M. Morales, U.R. Rodríguez-Mendoza, V. Lavín, Excited state dynamics in Yb^{3+}–Ho^{3+} doped fluoroindate glasses, Journal of Applied Spectroscopy 62 (1995) 865–871.